
Article:
Sun, S., Bai, J., Gu, J. et al. (7 more authors) (2024) Extraordinary mechanical properties and room-temperature magnetocaloric effects in spark plasma sintered all-d-metal Ni-Co-Mn-Ti alloy. Journal of Alloys and Compounds, 976. 173406. ISSN 0925-8388

https://doi.org/10.1016/j.jallcom.2023.173406

Extraordinary mechanical properties and room-temperature magnetocaloric effects in spark plasma sintered all-d-metal Ni-Co-Mn-Ti alloy

Shaodong Sun [1], [2] Jing Bai[1, 2, 4, *], Jianglong Gu[3], Keliang Guo[1], Nicola Morley[4], Qiuzhi Gao[2], Yudong Zhang[5], Claude Esling[5], Xiang Zhao[1], Liang Zuo[1]

[1]Key Laboratory for Anisotropy and Texture of Materials (Ministry of Education), School of Material Science and Engineering, Northeastern University, Shenyang 110819, China

[2]Key Laboratory of Dielectric and Electrolyte Functional Material Hebei Province, School of Resources and Materials, Northeastern University at Qinhuangdao, Qinhuangdao 066004, PR China

[3]State Key Laboratory of Metastable Materials Science and Technology, Yanshan University, Qinhuangdao 066004, China

[4]Department of Material Science and Engineering, University of Sheffield, Sheffield, S1 3JD, UK

[5]Laboratoire d'Étude des Microstructures et de Mécanique des Matériaux, UMR 7239, LEM3, CNRS, University of Lorraine, 57045 Metz, France

*Corresponding author: baijing@neuq.edu.cn

ABSTRACT

The all-d-metal Ni-Co-Mn-Ti Heusler alloy is a promising candidate for magnetic refrigeration application because of its considerable magnetocaloric effect and excellent mechanical properties. In this study, the influence of powder particle size on the martensitic transformation, magnetic and mechanical properties of $Ni_{37}Co_{13}Mn_{34}Ti_{16}$ spark plasma sintered samples have been investigated. It was found that the martensite transformation temperature was shifted to a higher value, while the mechanical properties decreased significantly with an increase in particle size. The sintered sample (S1) with a particle size of 0-15 μm exhibited enhanced characteristics such as thermal effect, magnetic and mechanical properties. The S1 martensitic transformation temperature occurred near ambient temperature, and the sample exhibited the maximum magnetic entropy changes as high as 37.53 $J \cdot kg^{-1} \cdot K^{-1}$ under a 5 T magnetic field. Moreover, the associated compressive fracture stress and strain were 2129 MPa and 27.78%, respectively, representing an 88.6% and 104.3% increase relative to the as-cast sample.

Keywords: Ni-Co-Mn-Ti all-d-metal Heusler alloy; Spark plasma sintering; Martensitic transformation; Magnetocaloric effect; Mechanical properties

1. Introduction

Refrigeration is an indispensable technology with far-ranging applications. Current refrigeration technology involves vapor-compression, which can be harmful to the environment. Magnetic refrigeration technology based on the magnetocaloric effect (MCE) is considered a preferable alternative to standard vapor-compression, and is anticipated to be incorporated in future solid-state refrigeration equipment[1-4]. The Ni-Mn-Ga/In-based Heusler alloys[5-8] have been the subject of magnetocaloric materials research for some time. Although Heusler alloys exhibit excellent magnetic and thermal properties, their inherent brittleness has hampered practical application.

In 2015, Wei et al. proposed an all-d-metal Ni-Mn-Ti alloy[9] and doped an appropriate amount of a fourth component (Co) into the ternary alloy to improve the magnetic properties and achieve magnetic-structure transition coupling. The results demonstrated that the alloy exhibited a maximum magnetic entropy change (ΔS_M) of 18 $J \cdot kg^{-1} \cdot K^{-1}$ with a high refrigerant capacity (267 $J \cdot kg^{-1}$) at a magnetic field of 5 T when the Co doping amount reached 15 at.%. These findings suggest that an all-d-metal Heusler alloy has significant potential as a magnetocaloric material. Subsequent studies have shown that the novel Ni-Mn-Ti-based Heusler alloy[10-13] can undergo martensitic transformation, exhibiting a large adiabatic temperature change under a stress field or magnetic field. Liu et al., in their exploration of $Ni_{36.5}Co_{13.5}Mn_{35}Ti_{15}$ annealed ribbons,[14] reported a peak magnetic entropy change of 24.9 $J \cdot kg^{-1} \cdot K^{-1}$ under a magnetic field change of 5 T. Liu et al. found that the reversible entropy changes can be substantially increased from 8.9 $J \cdot kg^{-1} \cdot K^{-1}$ to 24.1 $J \cdot kg^{-1} \cdot K^{-1}$ for magnetic field variations ranging from 0.01 T to 5 T in the case of $Ni_{37.5}Co_{12.5}Mn_{35}Ti_{15}$ alloy[15]. Guan et al. prepared a $Ni_{36.6}Co_{12.8}Mn_{34.7}Ti_{15.9}$ alloy[16] using directional solidification technology were the maximum magnetic entropies were 23.2 $J \cdot kg^{-1} \cdot K^{-1}$ and 28.1 $J \cdot kg^{-1} \cdot K^{-1}$ under a magnetic field change of 5 T and 7 T, respectively. The Ni-Mn-Ti-based Heusler alloy is recognized as one of the most promising elastocaloric and magnetocaloric materials. Therefore, a simple and efficient preparation process that can improve the multifunctional properties and end application value of Ni-Mn-Ti-based alloys is of appreciable practical significance.

Alloys prepared using the spark plasma sintered (SPS) method have shown excellent mechanical properties, notably high relative density, high hardness and toughness. Researchers have prepared different Ni-Mn-based alloys by SPS[17-25], and demonstrated enhanced mechanical performance.

Kuang et al. used SPS technology to prepare $Ni_{50}Mn_{34.7}In_{15.3}$ with different particle sizes[23]. The sintered powder exhibited a particle size of 15 μm with associated fracture stress and strain of 1800 MPa and 19.2%, respectively. The magnetic entropy change recorded for a particle size of 140 μm reached 18.8 $J \cdot kg^{-1} \cdot K^{-1}$ at a 5 T magnetic field. In addition, the magnetic entropy change was 17.1 $J \cdot kg^{-1} \cdot K^{-1}$ in the case of $Ni_{43.75}Mn_{37.5}In_{12.5}Co_{6.25}$ under a 5 T magnetic field. The fracture stress and strain were 1440 MPa and 14%, respectively, compared with 520 MPa and 10.5% for the as-cast sample, a response that may be attributed to grain refinement. The published results establish the SPS technique as an effective approach to improve mechanical properties while maintaining the magneto-caloric effect.

In this study, an all-d-metal $Ni_{37}Co_{13}Mn_{34}Ti_{16}$ alloy has been prepared by both arc melting and SPS technology, and the effects of particle size on the martensitic transformation, magnetic properties and mechanical properties of the sintered samples were systematically studied. The objective of this work is to produce a $Ni_{37}Co_{13}Mn_{34}Ti_{16}$ alloy with high magnetic entropy change and enhanced mechanical properties at near room temperature by adjusting the particle size.

2. Experimental methods

High-purity Ni (99.9%), Co (99.9%), Mn (99.5%), and Ti (99.9%) were used to prepare a $Ni_{37}Co_{13}Mn_{34}Ti_{16}$ ingot by arc melting under argon protection. More than 3% Mn was added due to the loss of Mn by evaporation during melting. The as-cast sample was annealed at 1223 K for 48 hours. Subsequently, high-pressure gas was used as an atomizing medium to crush the molten ingot into spherical powders. Following screening using a standard sieve, alloy powders with particle sizes of 0-15 μm, 15-53 μm, 53-106 μm, and 106-150 μm were obtained. SPS equipment was used to sinter the alloy powders at 1223 K for 15 min. The sintered samples were annealed at 1223 K for 6 hours to ensure uniformity of chemical composition. After annealing, all as-cast and sintered samples were immediately removed and quenched in water. The sintered samples are denoted as S1, S2, S3, and S4 in ascending order of powder particle sizes.

Sample microstructure and composition were analyzed using a scanning electron microscope (SEM, Zeiss SUPRA55) equipped with an energy dispersive spectrometer (EDS). A $3 \times 3 \times 5$ mm^3 rectangular sample was subjected to compression testing on a mechanical testing machine (AG-XPLUS100KN). The martensite transformation temperature was determined by differential scanning

calorimetry (DSC, Q100). Magnetism was measured using a quantum design physical property measurement system (PPMS) equipped with a vibrating sample magnetometer (VSM). The isothermal magnetization curve (M-H) was measured using the cyclic method where a discontinuous heating protocol was used to determine the ΔS_M value. In each measurement, the sample was first cooled to 150 K under zero field to ensure a complete martensite state, and then heated to the test temperature under zero field, and the M-H curves were recorded.

3. Results and discussion

3.1. Martensite transformation and microstructure

The feasibility of studying the Ni-Co-Mn-Ti alloy prepared by SPS was evaluated by testing and comparing the density, martensitic transformation and microstructure of SPS samples with the as-cast sample. The density of the sintered samples and the relative density with respect to the as-cast sample are shown in Fig. 1(a). The density of the as-cast sample was 7.166 g·cm^{-3}, and the density of the SPS samples decreased from 7.09 g·cm^{-3} to 7.07 g·cm^{-3}, with a relative density decrease from 98.96% to 98.66% as powder particle size decreased. This suggests that the $Ni_{37}Co_{13}Mn_{34}Ti_{16}$ alloy sintered by the SPS technique was in a dense state with little porosity. The DSC curves of the as-cast and SPS samples with different powder particle sizes are presented in Fig. 1(b). The characteristic martensitic transformation temperatures (M_s, M_f, A_s, A_f) were determined using the tangent method[24], where the transformation thermal hysteresis is defined by $\Delta T_{hys} = \left[\left(A_s + A_f\right) - \left(M_s + M_f\right)\right]/2$. The variation of martensite transformation temperature and thermal hysteresis for the as-cast and sintered samples is illustrated in Fig. 1(c). The enthalpy change (ΔH) and entropy change ($\Delta S = \Delta H/T_0,\ T_0 = \left(A_s + A_f\right)/2$) of the samples are given in Table 1. It can be seen (Fig. 1(b)) that the sintered samples with different particle sizes exhibit the same typical endothermic and exothermic peaks as the as-cast sample during the martensitic transformation. The martensitic transition temperatures of the sintered samples were shifted to higher values relative to the as-cast sample, with the transition temperature close to ambient temperature. This proximity to room temperature is favorable for the generation of the magnetocaloric effect (MCE) in practical applications. In addition, variations in the powder particle size significantly influenced the martensitic transformation temperature. With an increase in particle size, the DSC curves of the sintered samples were shifted to higher temperatures, with a resultant reduction in the heat absorbed and released by the sintered samples. The peak width was

wider as a consequence of this shift. Moreover, the temperature range of the martensitic transformation ΔT（$\Delta T = M_s - M_f$）exhibited a marked increase from 20 K to 61 K, demonstrating that an increased powder size resulted in a less obvious martensitic transformation. The maximum thermal hysteresis observed for the S1 sample was 19.8 K. Previous studies have reported that the martensitic transformation can be suppressed when the grain size is reduced to a certain threshold[23, 26].

The microstructure and morphology of the powder and sintered samples are shown in Fig. 1(d) and (e), respectively. The boundaries between particles are clearly seen in Fig. 1(e). Notably, no evident defects, such as large pores and intergranular cracks, were observed in the sintered samples (S1-S4), confirming their high relative density. According to SEM image statistics, the median particle sizes of the sintered samples are 10.535 μm, 39.305 μm, 80.335 μm and 132.205 μm for S1-S4, respectively. The grain size of the sintered sample is consistent with that of the original powder size. In the sintering process, heat and pressure are transmitted between particles. As a result, in the sintered sample, all particles are deformed and occupy the space between them, resulting in the sintered sample with a relatively high density[27].

The actual compositions of the as-cast sample and sintered samples are provided in Table 1. The composition of all sintered samples is close to that of the as-cast sample, which is approximately the nominal composition of $Ni_{37}Co_{13}Mn_{34}Ti_{16}$.

Samples	Actual composition				$\triangle H$/ J·g^{-1}	$\triangle S$/ J·K^{-1}·kg^{-1}
	Ni/ at. %	Co/ at. %	Mn/ at. %	Ti/ at. %		
As-cast	36.64	13.20	34.27	15.87	9.8	37.2
S1	37.16	12.83	34.65	15.36	12.1	40.5
S2	37.24	12.91	34.50	15.35	11.9	39.3
S3	36.79	13.45	34.51	15.26	12.3	39.6
S4	36.88	13.12	34.19	15.81	10.5	33.1

Table 1. Actual composition, ΔH and ΔS of the as-cast and sintered samples.

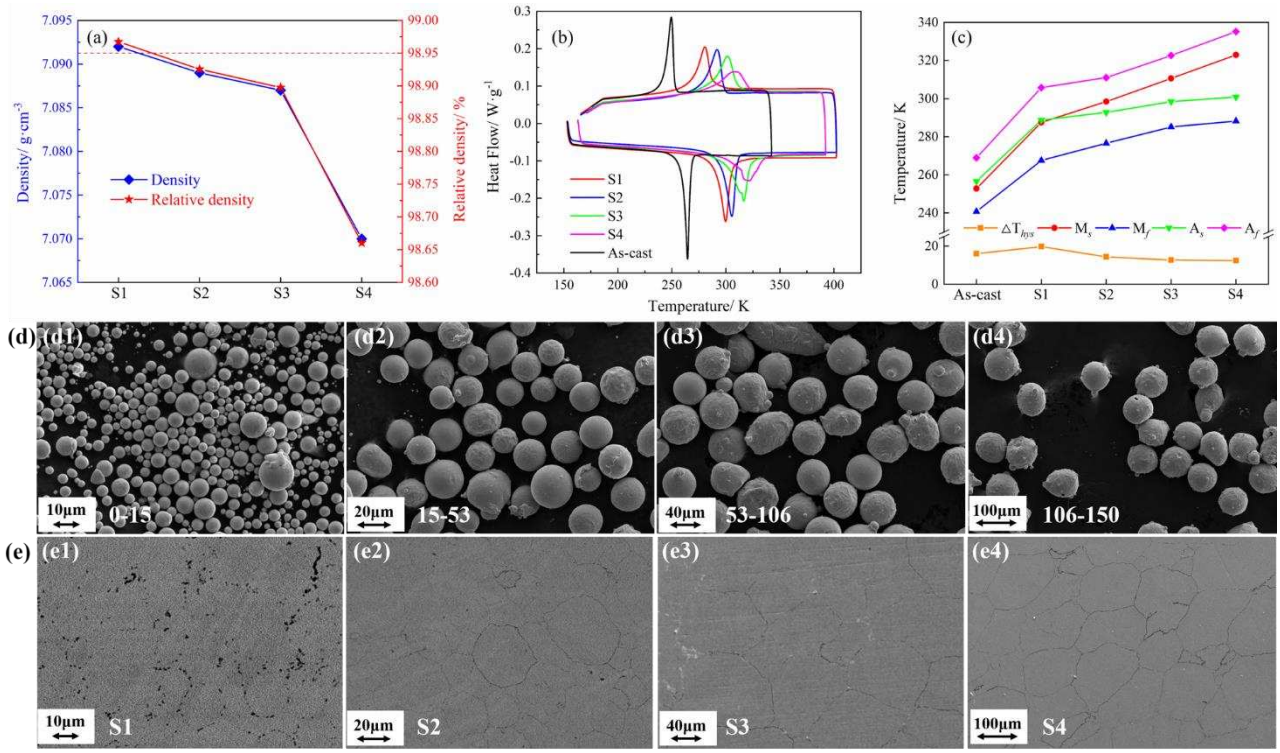

Fig. 1. (a) Density and relative density of sintered samples. (b) DSC curves of the as-cast and sintered samples. (c) Variations in the martensite transformation temperature and thermal hysteresis. (d) and (e) SEM of the powders and corresponding sintered samples.

3.2. Mechanical properties

Compression stress-strain tests were performed to assess the mechanical properties of as-cast and SPS samples. The room temperature compressive stress-strain curves of both sintered and as-cast $Ni_{37}Co_{13}Mn_{34}Ti_{16}$ are presented in Fig. 2(a). The compressive fracture stress and strain of all the sintered samples, regardless of particle size, exhibited a clear enhancement relative to the as-cast sample. With a decrease in particle size, the fracture stress-strain of the sintered sample increased. The compressive fracture stress and strain of the as-cast sample were 1128.93 MPa and 13.6%, respectively. The compressive fracture stress and strain of S1 were 2136.92 MPa and 27.78%, respectively, representing a distinct improvement (89.29% and 105.17%) compared with the as-cast sample.

The remarkable mechanical properties exhibited by the sintered samples can be attributed to fine grain strengthening. The reduction in grain size in the sintered sample results in an increased number of grain boundaries, effectively impeding crack propagation. Consequently, this fine grain structure enhances the overall mechanical properties. In addition to the influence of grain size, the

microstructure also plays a significant role in determining the mechanical properties of the sintered samples. The sintered sample is composed of austenite and martensite phases at room temperature. The austenite contributes to plasticity and ductility, while the martensite is a hard and brittle phase. The relative content of each phase in the sintered sample determines the mechanical properties. All sintered samples underwent a homogenization annealing treatment to eliminate residual stress during sintering. The sintered samples with different particle sizes did not show any obvious defects such as cracks, as can be assessed from the images provided in Fig. 1(e). The combined effect of the factors noted above serves to appreciably improve the mechanical properties of the SPS samples.

The compressive stress-strain curves of sample S1 sample (solid red line) shown in Fig. 2(b) can be compared with the response for Ni-Mn-Ti-based alloys[10, 28, 29] and other Ni-Mn-based magnetic shape memory alloys(MSMAs) prepared using the SPS technique[17, 18, 20, 21, 23, 24] . Both $Ni_{48.8}Mn_{29.8}Ga_{21.5}$[17] and $Ni_{50}Mn_{29}Ga_{21}$[18] are characterized by a compressive fracture strain close to the S1 sample, but the compressive fracture stress was ca. 400 MPa lower. The $Ni_{45}Co_5Mn_{36.7}In_{13.3}$ and $Ni_{50}Mn_{34.7}In_{15.3}$ alloys exhibit considerable compressive fracture stress, but the fracture strain differed by ca. 10% compared with S1. Furthermore, the compressive fracture stress and strain of S1 were nearly twice that recorded for the directionally solidified Ni-Mn-Ti sample[10] and the as-cast Ni-Co-Mn-Ti sample[28, 29] . The results establish that S1, fabricated using the SPS process, exhibits superior mechanical properties to others Ni-Mn based MSMAs.

In order to clarify the fracture mechanism of the as-cast and sintered samples, the fracture morphologies were examined by SEM. The image presented in Fig. 2(c) illustrates a typical intergranular fracture and cleavage fracture in the as-cast sample, indicating a mixed fracture mode. In contrast, the morphologies shown in Figs. 2(d)-(g) reveal the surface fracture morphology associated with samples S1-S4, which was primarily cleavage fracture. The growth path of the cleavage crack can be seen in Fig. 2(f), which reveals the fracture mechanism associated with the sintered samples. When subjected to external stress, cracks initiate within the grain of the sintered sample. These cracks traverse the boundaries of neighboring particles, generating new cracks on adjacent particles from which the cracks propagate and ultimately extend throughout the entire particle. The crack source originates at a central point in the particle and spreads outward in a fan-shaped pattern, forming a cleavage sector (indicated by the circular dotted line in Fig. 2 (f)). As the particle size increases, at the same sintering pressure the binding force between particle boundaries

decreases, leading to inter-particle fracture (Fig. 2(g)). It can be seen from Fig. 2(c) that the particle size of the as-cast sample is about 187 μm. Fig. 2(h) displays the relationship between particle size and mechanical properties. As the particle size decreases, there is a notable upward trend in both the compressive stress and strain, which proves the Hall-Petch relationship.

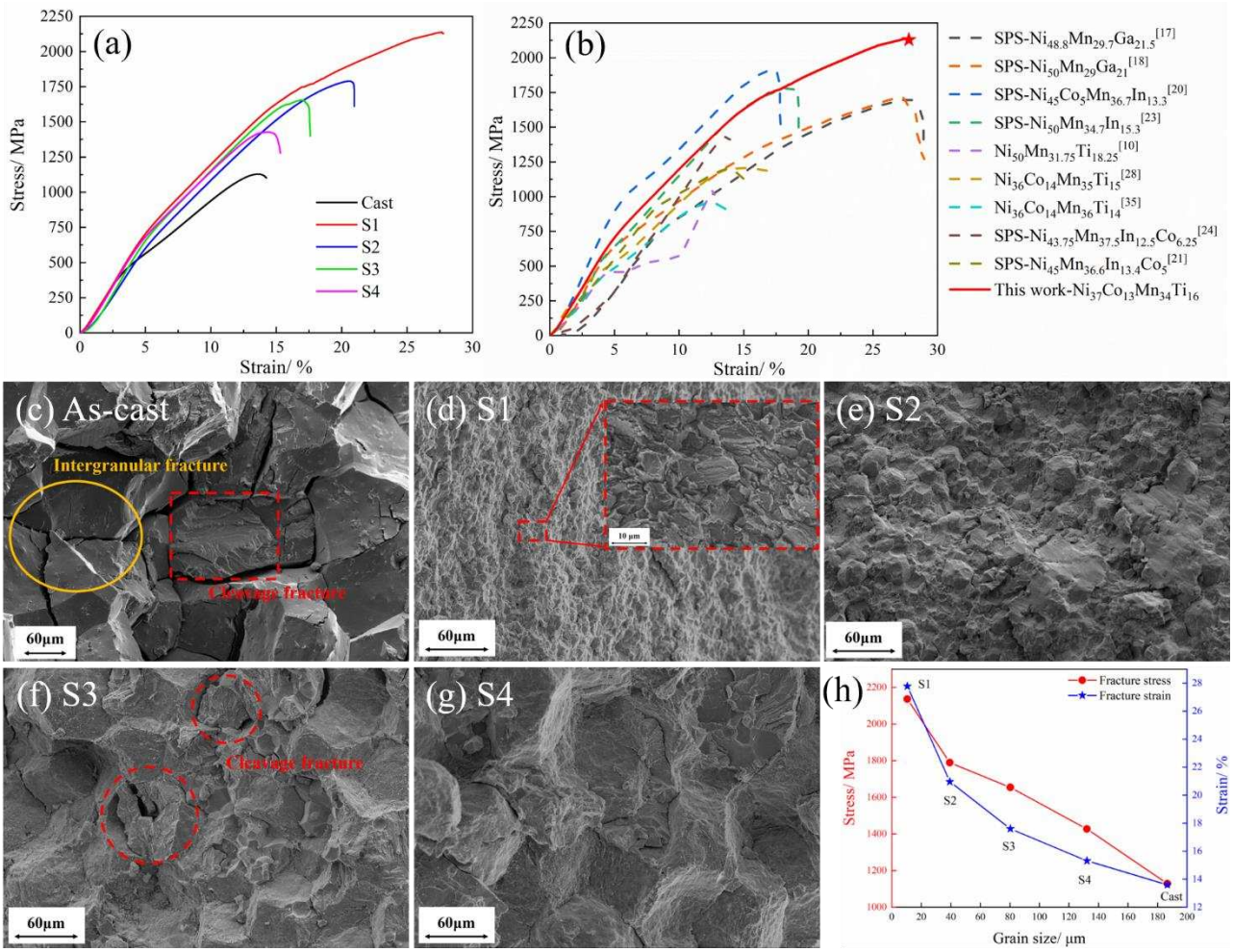

Fig. 2. (a) Stress-strain curves of as-cast and sintered samples. (b) Comparison of the mechanical properties of S1 and other Ni-Mn based samples. (c)-(g) Fracture morphologies of as-cast and sintered samples with different powder sizes. (h) The relationship between the mechanical properties and grain size.

3.3. Magnetic properties

Considering the isothermal entropy change during martensite transformation and the mechanical property of SPS samples, S1 was selected to determine the magnetization-temperature (M-T) and isothermal magnetic hysteresis (M-H) curves. The M-T curves for S1 under 0.05 T and 5 T magnetic fields are presented in Fig. 3, showing a typical magnetic-structural transition from ferromagnetic austenite to weakly magnetic martensite. The characteristic temperature of martensitic transition

under a 5 T magnetic field shows a distinct shift to a lower temperature compared with the 0.05 T magnetic field. This response suggests that the higher magnetic field is more conducive to the stability of the austenitic phase with a consequent shift of the martensitic phase transition to a lower temperature[23, 28] . The characteristic temperature of the martensitic transition under a magnetic field was determined using the tangent method, and the corresponding values are given in Table 2.

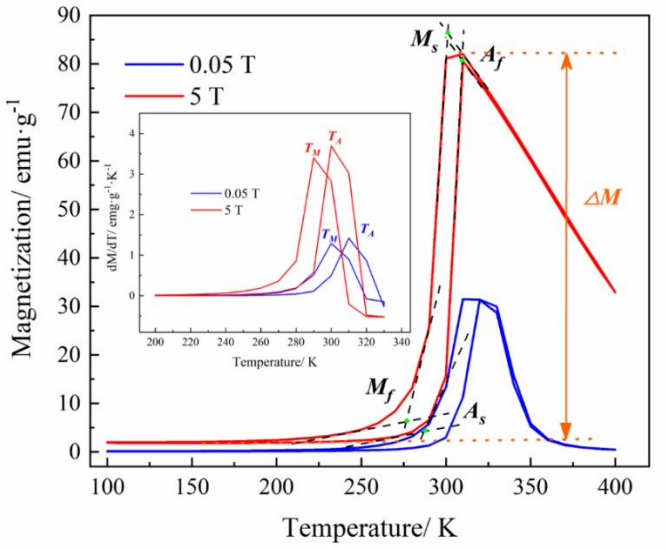

Fig. 3. M-T curves of S1 under 0.05 and 5 T magnetic fields. The inset shows the relationship between dM/dT and T.

As a basic parameter that characterizes magnetically controlled multifunctional material, the magnetization difference (ΔM) between austenite and martensite during the martensitic transformation was determined from the entries in Fig. 3. A larger ΔM signifies a favorable magnetic control functionality. The ΔM of S1 at a 5 T magnetic field was 79.98 emu·g^{-1}, similar to the current Ni-Mn-based alloy[30-34] . The difficulty of the magnetic field-induced inverse martensitic transition is reflected in the dM/dT values[35] , as illustrated in Fig. 3. T_M and T_A represent the peak temperatures of martensite transformation and reverse martensite transformation, respectively, which are given in Table 2. In the case of S1, the change in T_A was −9.99 K, corresponding to a dM/dT value of − 2.02 K/T when the magnetic field was varied from 0.05 T to 5 T.

Sample	H/ T	M_s/ K	M_f/ K	A_s/ K	A_f/ K	T_A/ K	T_M/ K	ΔM/ emu·g^{-1}
S1	0.05	316.90	286.30	297.73	320.08	309.95	299.97	31.51
	5	300.38	276.44	288.10	310.32	300.09	290.01	82.05

Table 2. Characteristic temperatures of martensitic transformation of S1 under a magnetic field (0.05 T and 5 T).

The MCE is a property of a magnetic material which allows absorption and release of heat when

subjected to an external magnetic field, and it can be characterized by the associated magnetic entropy change (ΔS_M). A series of M-H curves for S1 are shown in Fig. 4(a) in the magnetic field range 0-5 T and temperature range 260 K-312.5 K. The M-H measurements were conducted at a temperature interval of 5 K between 260 K and 300 K and a 2.5 K interval between 300 K and 312.5 K.

Magnetization of the complete martensite phase at 150 K was measured, and appears as the black curve in Fig. 4(a). When the magnetic field was increased to 5 T, the measured magnetization of S1 was 1.92 emu·g^{-1}, indicating the weakly magnetic nature of martensite, which is consistent with the M-T curve in Fig. 3. As shown in Fig. 4(a), the magnetic saturation of S1 gradually increased at higher temperatures. At 295 K, the curves do not overlap, indicating the occurrence of a magnetic field-induced martensitic transition. At 300 K, a more pronounced reversible magnetic field-induced martensitic transition can be observed. The results establish a typical magneto-structural coupling transformation from weakly magnetic martensite to ferromagnetic austenite within the temperature range of 270-312.5 K.

The series of isothermal-magnetization curves in Fig. 4(a) were subjected to Maxwell's equation (1-1)[24] . The resultant relationships between temperature and ΔS_M for S1 in the magnetic field-induced inverse martensitic are shown in Fig. 4(b).

$$\Delta S_M(T,\ H)_{\Delta H} = S(T,\ H) - S(T,\ 0) = \int_0^H (\partial M / \partial H)_H dH \qquad (1\text{-}1)$$

In equation (1-1), M represents the magnetization intensity of the sample corresponding to the increase of the magnetic field (H) at temperature (T).

As can be seen in Fig. 4(b), S1 exhibited a maximum ΔS_M of 37.53 J·kg^{-1}·K^{-1} at 307.5 K under a 5 T magnetic field. It should be noted that an abnormal peak (ΔS_M of 11.95 J·kg^{-1}·K^{-1}) at 300 K has also been observed in previous studies[28]. This peak can broaden the operating temperature range and is a beneficial feature of the alloy magnetothermal effect. The maximum ΔS_M recorded in this work is presented in Fig. 4(c) and can be compared with values reported for Ni-Co-Mn-Ti alloys[9, 14, 16, 28, 29, 36-41] and other Ni-Mn based alloys[23] under a 5 T magnetic field. The ΔS_M of S1 is at a high level, indicating an enhanced ability to absorb and release heat under the action of a magnetic field. This confirms that SPS delivers high efficiency in fabricating an all-d-metal Ni-Co-Mn-Ti Heusler alloy with exceptional magnetocaloric effect performance that is a promising candidate for magnetic refrigeration applications.

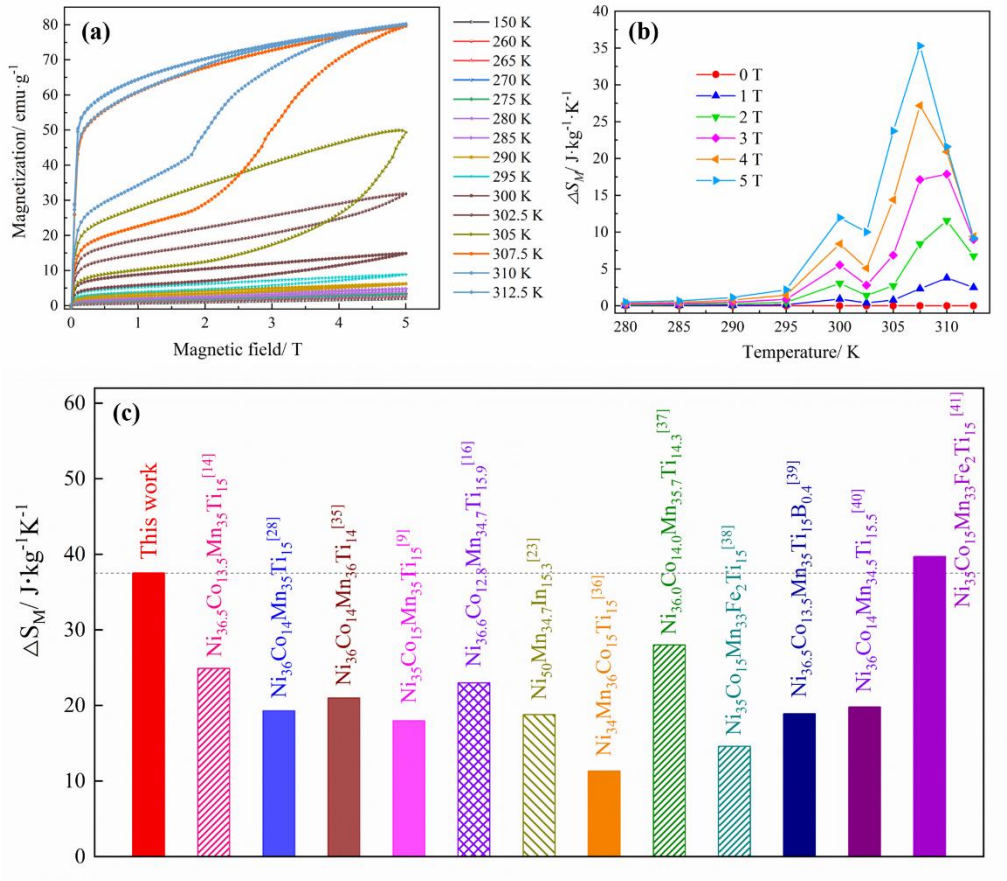

Fig. 4. (a) Isothermal magnetization curves of S1 at 150 K and 260-312.5 K. (b) Relationship between ΔS_M and temperature for S1 under a 0-5 T magnetic field. (c) Comparison of the ΔS_M values generated for S1 and related alloy systems under a 5 T magnetic field.

4. Conclusions

The sintered samples with different powder particle sizes exhibit excellent formability with a relative density greater than 98.6%. The sintered samples have few obvious defects, such as unfused particle boundaries. The characteristic temperature of martensite transformation and mechanical properties increase notably with a decrease in powder size. The compressive fracture stress and strain of the as-cast sample are 1128.93 MPa and 13.6%, respectively. The compressive fracture stress and strain of S1 are 2129 MPa and 27.78%, respectively, 88.6% and 104.3% higher than the as-cast sample. Moreover, the mechanical properties of S1 are superior to most of other NiMn-based SMAs. The maximum ΔS_M exhibited by S1 under a 5 T magnetic field is 37.53 $J \cdot kg^{-1} \cdot K^{-1}$, which is at a high level among NiMn-based alloys.

Acknowledgments

This work is financially supported by the National Natural Science Foundation of China (Grant No. 51771044), the Natural Science Foundation of Hebei Province (No. E2019501061), the Performance subsidy fund for Key Laboratory of Dielectric and Electrolyte Functional Material Hebei (No. 22567627H), the Fundamental Research Funds for the Central Universities (No. N2223025), and the Programme of Introducing Talents of Discipline Innovation to Universities 2.0 (the 111 Project of China 2.0, No. BP0719037). This project is supported by the China Scholarship Council (CSC).

Author contributions

Zuo L and Bai J conceived and coordinated the project, and were responsible for the infrastructure and project direction. Sun SD and Gu JL conducted the experiments. Zhang YD, Esling C, and Zhao X contributed to data analysis and interpretation. Sun SD wrote the manuscript. All authors contributed to the general discussion.

Conflict of interest

The authors declares that they have no conflict of interest.

References

[1] J. Lyubina, O. Gutfleisch, M. D. Kuz'min, M. Richter, La(Fe,Si)$_{13}$-based magnetic refrigerants obtained by novel processing routes, J. Magn. Magn. Mater., 320(2008)2252-2258, https://doi.org/10.1016/j.jmmm.2008.04.116

[2] D. Liu, M. Yue, J. X. Zhang, T. M. McQueen, J. W. Lynn, X. L. Wang, Y. Chen, J. Y. Li, R. J. Cava, X. B. Liu, Z. Altounian, Q. Huang, Origin and tuning of the magnetocaloric effect in the magnetic refrigerant $Mn_{1.1}Fe_{0.9}(P_{0.8}Ge_{0.2})$, Phys. Rev. B, 79(2009)https://doi.org/10.1103/PhysRevB.79.014435

[3] B. G. Shen, J. R. Sun, F. X. Hu, H. W. Zhang, Z. H. Cheng, Recent progress in exploring magnetocaloric materials, Adv. Mater., 21(2009)4545-4564, https://doi.org/10.1002/adma.200901072

[4] V. Franco, J. S. Blázquez, B. Ingale, A. Conde, The magnetocaloric effect and magnetic refrigeration near room temperature: materials and models, Annu. Rev. Mater. Res., 42(2012)305-342, https://doi.org/10.1146/annurev-matsci-062910-100356

[5] Y. J. Huang, Q. D. Hu, N. M. Bruno, J.-H. Chen, I. Karaman, J. H. Ross, J. G. Li, Giant elastocaloric effect in directionally solidified Ni–Mn–In magnetic shape memory alloy, Scr. Mater., 105(2015)42-45, https://doi.org/10.1016/j.scriptamat.2015.04.024

[6] X. X. Zhang, M. F. Qian, R. Z. Su, L. Geng, Giant room-temperature inverse and conventional magnetocaloric effects in Ni–Mn–In alloys, Mater. Lett., 163(2016)274-276, https://doi.org/10.1016/j.matlet.2015.10.076

[7] M. V. McLeod, A. K. Giri, B. A. Paterson, C. L. Dennis, L. Zhou, S. C. Vogel, O. Gourdon, H. M. Reiche, K. C. Cho, Y. H. Sohn, R. D. Shull, B. S. Majumdar, Magnetocaloric response of non-stoichiometric Ni_2MnGa alloys and the influence of crystallographic texture, Acta. Mater., 97(2015)245-256, https://doi.org/10.1016/j.actamat.2015.06.059

[8] S. Dey, R. K. Roy, M. Ghosh, A. Basu Mallick, A. Mitra, A. K. Panda, Enhancement in magnetocaloric properties of NiMnGa alloy through stoichiometric tuned phase transformation and magneto-thermal transitions, J. Magn. Magn. Mater., 439(2017)305-311, https://doi.org/10.1016/j.jmmm.2017.04.088

[9] Z. Y. Wei, E. K. Liu, J. H. Chen, Y. Li, G. D. Liu, H. Z. Luo, X. K. Xi, H. W. Zhang, W. H. Wang, G. H. Wu, Realization of multifunctional shape-memory ferromagnets in all-d-metal Heusler phases, Appl. Phys. Lett., 107(2015)022406, https://doi.org/10.1063/1.4927058

[10] H. L. Yan, L. D. Wang, H. X. Liu, X. M. Huang, N. Jia, Z. B. Li, B. Yang, Y. D. Zhang, C. Esling, X. Zhao, L. Zuo, Giant elastocaloric effect and exceptional mechanical properties in an all-d-metal Ni–Mn–Ti alloy: Experimental and ab-initio studies, Mater. Des., 184(2019)108180, https://doi.org/10.1016/j.matdes.2019.108180

[11] D. Y. Cong, W. X. Xiong, A. Planes, Y. Ren, L. Manosa, P. Y. Cao, Z. H. Nie, X. M. Sun, Z. Yang, X. F. Hong, Y. D. Wang, Colossal elastocaloric effect in ferroelastic Ni-Mn-Ti alloys, Phys. Rev. Lett., 122(2019)255703, https://doi.org/10.1103/PhysRevLett.122.255703

[12] Z. Y. Wei, W. Sun, Q. Shen, Y. Shen, Y. F. Zhang, E. K. Liu, J. Liu, Elastocaloric effect of all-d-metal Heusler NiMnTi(Co) magnetic shape memory alloys by digital image correlation and infrared thermography, Appl. Phys. Lett., 114(2019)101903, https://doi.org/10.1063/1.5077076

[13] Z. Q. Guan, J. Bai, J. L. Gu, X. Z. Liang, D. Liu, X. J. Jiang, R. K. Huang, Y. D. Zhang, C. Esling, X. Zhao, L. Zuo, First-principles investigation of B2 partial disordered structure, martensitic transformation, elastic and magnetic properties of all-d-metal Ni-Mn-Ti Heusler alloys, J. Mater. Sci. Technol., 68(2021)103-111, https://doi.org/10.1016/j.jmst.2020.08.002

[14] K. Liu, S. C. Ma, C. C. Ma, X. Q. Han, K. Yu, S. Yang, Z. S. Zhang, Y. Song, X. H. Luo, C. C. Chen, S. U. Rehman, Z. C. Zhong, Martensitic transformation and giant magneto-functional properties in all-d-metal Ni-Co-Mn-Ti alloy ribbons, J. Alloys. Compd., 790(2019)78-92, https://doi.org/10.1016/j.jallcom.2019.03.173

[15] Y. Liu, A. D. Xiao, T. Z. Yang, Z. T. Xu, X. L. Zhou, T. Y. Ma, Enhancing reversible entropy change of all-d-metal $Ni_{37.5}Co_{12.5}Mn_{35}Ti_{15}$ alloy by multiple external fields, Scr. Mater., 207(2022)114303, https://doi.org/10.1016/j.scriptamat.2021.114303

[16] Z. Q. Guan, J. Bai, S. D. Sun, J. L. Gu, X. Z. Liang, Y. D. Zhang, C. Esling, X. Zhao, L. Zuo, Extraordinary mechanical properties and successive caloric effects with ultrahigh cyclic stability in directionally solidified $Ni_{36.6}Co_{12.8}Mn_{34.7}Ti_{15.9}$ alloy, Appl. Mater. Today, 29(2022)101634, https://doi.org/10.1016/j.apmt.2022.101634

[17] X. H. Tian, J. H. Sui, X. Zhang, X. Feng, W. Cai, Martensitic transformation, mechanical property and magnetic-field-induced strain of Ni–Mn–Ga alloy fabricated by spark plasma sintering, J. Alloys. Compd., 509(2011)4081-4083, https://doi.org/10.1016/j.jallcom.2011.01.001

[18] X. H. Tian, J. H. Sui, X. Zhang, X. H. Zheng, W. Cai, Grain size effect on martensitic transformation, mechanical and magnetic properties of Ni–Mn–Ga alloy fabricated by spark plasma sintering, J. Alloys. Compd., 514(2012)210-213, https://doi.org/10.1016/j.jallcom.2011.11.077

[19] P. Ochin, A. V. Gilchuk, G. E. Monastyrsky, Y. Koval, A. A. Shcherba, S. N. Zaharchenko, Martensitic transformation in spark plasma sintered compacts of Ni-Mn-Ga powders prepared by spark erosion method in cryogenic liquids, Mater. Sci. Forum, 738-739(2013)451-455, https://doi.org/10.4028/www.scientific.net/MSF.738-739.451

[20] B. Tian, D. C. Ren, Y. X. Tong, F. Chen, L. Li, Y. F. Zheng, Microstructure, phase transformation and mechanical property of Ni-Co-Mn-In alloy prepared by spark plasma sintering, Mater. Sci. Forum, 815(2015)222-226, https://doi.org/10.4028/www.scientific.net/MSF.815.222

[21] Y. Feng, H. Chen, F. Xiao, X. H. Bian, P. Wang, Improvement of mechanical property and large shape recovery of sintered $Ni_{45}Mn_{36.6}In_{13.4}Co_5$ alloy, J. Alloys. Compd., 765(2018)264-270, https://doi.org/10.1016/j.jallcom.2018.06.244

[22] E. Matyja, K. Prusik, M. Zubko, G. Dercz, K. Glowka, Structure of the Ni-Co-Mn-In alloy obtained by mechanical alloying and sintering, J. Alloys. Compd., 801(2019)529-535, https://doi.org/10.1016/j.jallcom.2019.06.079

[23] Y. F. Kuang, Z. R. Ai, B. Yang, X. W. Hao, Z. B. Li, H. L.Yan, Y. D.Zhang, C. Esling, X. Zhao, L. Zuo, Simultaneously achieved good mechanical properties and large magnetocaloric effect in spark plasma sintered Ni-Mn-In alloys, Intermetallics, 124(2020)106868, https://doi.org/10.1016/j.intermet.2020.106868

[24] J. Bai, D. Liu, J. L. Gu, X. J. Jiang, X. Z. Liang, Z. Q. Guan, Y. D. Zhang, C. Esling, X. Zhao, L. Zuo, Excellent mechanical properties and large magnetocaloric effect of spark plasma sintered Ni-Mn-In-Co alloy, J. Mater. Sci. Technol., 74(2021)46-51, https://doi.org/10.1016/j.jmst.2020.10.011

[25] J. D. Navarro-García, J. L. Sánchez Llamazares, J. P. Camarillo-Garcia, Synthesis of highly dense spark plasma sintered magnetocaloric Ni-Mn-Sn alloys from melt-spun ribbons, Mater. Lett., 295(2021)129857, https://doi.org/10.1016/j.matlet.2021.129857

[26] J. Liu, M. X. Xia, Y. L. Huang, H. X. Zheng, J. G. Li, Effect of annealing on the microstructure and martensitic transformation of magnetic shape memory alloys CoNiGa, J. Alloys. Compd., 417(2006)96-99, https://doi.org/10.1016/j.jallcom.2005.09.026

[27] C. Velmurugan, V. Senthilkumar, K. Biswas, S. Yadav, Densification and microstructural evolution of spark plasma sintered NiTi shape memory alloy, Adv. Powder Technol., 29(2018)2456-2462, https://doi.org/10.1016/j.apt.2018.06.026

[28] Z. Q. Guan, X. J. Jiang, J. L. Gu, J. Bai, X. Z. Liang, H. L. Yan, Y. D. Zhang, C. Esling, X. Zhao, L. Zuo, Large magnetocaloric effect and excellent mechanical properties near room temperature in Ni-Co-Mn-Ti non-textured polycrystalline alloys, Appl. Phys. Lett., 119(2021)051904, https://doi.org/10.1063/5.0058609

[29] Z. Q. Guan, J. Bai, Y. Zhang, J. L. Gu, X. J. Jiang, X. Z. Liang, R. K. Huang, Y. D. Zhang, C. Esling, X. Zhao, L. Zuo, Revealing essence of magnetostructural coupling of Ni-Co-Mn-Ti alloys by first-principles calculations and experimental verification, Rare Met., 41(2022)1933-

1947, https://doi.org/10.1007/s12598-021-01947-2

[30] X. Z. Liang, J. Bai, J. L. Gu, H. L. Yan, Y. D. Zhang, C. Esling, X. Zhao, L. Zuo, Probing martensitic transformation, kinetics, elastic and magnetic properties of $Ni_{2-x}Mn_{1.5}In_{0.5}Co_x$ alloys, J. Mater. Sci. Technol., 44(2020)31-41, https://doi.org/10.1016/j.jmst.2020.01.034

[31] Z. Z. Li, Z. B. Li, Y. Z. Lu, X. Lu, L. Zuo, Enhanced elastocaloric effect and refrigeration properties in a Si-doped Ni-Mn-In shape memory alloy, J. Mater. Sci. Technol., 117(2022)167-173, https://doi.org/10.1016/j.jmst.2021.11.051

[32] F. Q. Zhang, K. Westra, Q. Shen, I. Batashev, A. Kiecana, N. van Dijk, E. Brück, The second-order magnetic phase transition and magnetocaloric effect in all-d-metal NiCoMnTi-based Heusler alloys, J. Alloys. Compd., 906(2022)164337, https://doi.org/10.1016/j.jallcom.2022.164337

[33] Y. H. Qu, D. Y. Cong, Z. Chen, W. Y. Gui, X. M. Sun, S. H. Li, L. Ma, Y. D. Wang, Large and reversible inverse magnetocaloric effect in $Ni_{48.1}Co_{2.9}Mn_{35.0}In_{14.0}$ metamagnetic shape memory microwire, Appl. Phys. Lett., 111(2017)192412, https://doi.org/10.1063/1.5000450

[34] J. Liu, T. Gottschall, K. P. Skokov, J. D. Moore, O. Gutfleisch, Giant magnetocaloric effect driven by structural transitions, Nat. Mater., 11(2012)620-626, https://doi.org/10.1038/nmat3334

[35] H. Neves Bez, A. K. Pathak, A. Biswas, N. Zarkevich, V. Balema, Y. Mudryk, D. D. Johnson, V. K. Pecharsky, Giant enhancement of the magnetocaloric response in Ni–Co–Mn–Ti by rapid solidification, Acta. Mater., 173(2019)225-230, https://doi.org/10.1016/j.actamat.2019.05.004

[36] N. u. Hassan, I. A. Shah, M. Jelani, M. Naeem, S. Riaz, S. Naseem, F. Xu, Z. Ullah, Effect of Ni-Mn ratio on structural, martensitic and magnetic properties of Ni-Mn-Co-Ti ferromagnetic shape memory alloys, Mater. Res. Lett., 5(2018)086102, https://doi.org/10.1088/2053-1591/aad124

[37] K. Liu, X. Q. Han, K. Yu, C. C. Ma, Z. S. Zhang, Y. Song, S. C. Ma, H. Zeng, C. C. Chen, X. H. Luo, S. U. Rehman, Z. C. Zhong, Magnetic-field-induced metamagnetic reverse martensitic transformation and magnetocaloric effect in all-d-metal $Ni_{36.0}Co_{14.0}Mn_{35.7}Ti_{14.3}$ alloy ribbons, Intermetallics, 110(2019)106472, https://doi.org/10.1016/j.intermet.2019.106472

[38] Y. Li, L. Qin, S. Y. Huang, L. W. Li, Enhanced magnetocaloric performances and tunable martensitic transformation in $Ni_{35}Co_{15}Mn_{35-x}Fe_xTi_{15}$ all-d-metal Heusler alloys by chemical and physical pressures, Sci. China Mater., 65(2021)486-493, https://doi.org/10.1007/s40843-021-1747-3

[39] F. Q. Zhang, I. Batashev, N. van Dijk, E. Bruck, Reduced hysteresis and enhanced giant magnetocaloric effect in B-doped all-d-metal Ni-Co-Mn-Ti-based Heusler materials, Phys. Rev. Appl., 17(2022)054032, https://doi.org/10.1103/PhysRevApplied.17.054032

[40] S. Samanta, S. Chatterjee, S. Ghosh, K. Mandal, Large reversible magnetocaloric effect and magnetoresistance by improving crystallographic compatibility condition in Ni(Co)-Mn-Ti all-d-metal Heusler alloys, Phys. Rev. Mater., 6(2022)094411, https://doi.org/10.1103/PhysRevMaterials.6.094411

[41] Y. Li, L. Qin, H. G. Zhang, L. W. Li, Tailored martensitic transformation and enhanced magnetocaloric effect in all-d-metal $Ni_{35}Co_{15}Mn_{33}Fe_2Ti_{15}$ alloy ribbons, Chin. Phys. B, 31(2022)087103, https://doi.org/10.1088/1674-1056/ac6edf